Polarization switching versus optical bistability: Experimental observations for a $J_{\text{lower}}=1$ to $J_{\text{upper}}=0$ transition in a Fabry-Perot cavity

C. Parigger
Department of Physics, University of Otago, Dunedin, New Zealand

P. Hannaford
Commonwealth Scientific and Industrial Research Organization, Division of Chemical Physics, Clayton, Victoria, 3168, Australia

W. J. Sandle*
Joint Institute for Laboratory Astrophysics, University of Colorado and National Bureau of Standards, Boulder, Colorado 80309-0440

(Received 20 March 1986)

Experiments on the steady-state, nonlinear behavior of the $^7F_1$-$^7F_0^o$ 570.68-nm transition of atomic samarium in a laser-driven, near-concentric Fabry-Perot cavity are reported. For zero applied magnetic field, only simple optical bistability, symmetric in both σ^+ and σ^- transmitted polarizations, is observed for a linearly polarized excitation beam. However, for a magnetic field applied parallel to the propagation direction, polarization-sensitive switching appears, with lowest power threshold near the edge of the Doppler-broadened region. Subsidiary measurements of atomic parameters are also given to enable the transition to be experimentally well characterized.

I. INTRODUCTION

The role of specifically *atomic physics* effects in optical bistability[1] (OB) and related switching studies has, in comparison with other aspects of this rapidly growing field, been rather neglected. Yet study of these effects is an inescapable part of experimentation with atoms in nonlinear optics. Furthermore, new optical switching phenomenologies with important theoretical and potential practical implications can be expected. We have, in fact, recently presented new, preliminary experimental and theoretical evidence for such an effect: *magnetically induced polarization switching*[2] (MIPS). This effect arises from competition between longitudinal optical pumping and laser-induced lower-level coherence for atoms in a laser-driven optical cavity. The system reported, the $J=1$ (lower) to $J'=0$ (upper) $^7F_1$-$^7F_0^o$ 570.68-nm transition Sm I in a Fabry-Perot cavity, does *not* show other than conventional OB for zero applied magnetic field. However, when a field of order of magnitude sufficient to remove the lower-level degeneracy is applied parallel to the propagation direction, polarization-sensitive switching[3-10] (PS) occurs in which a strong asymmetry develops between σ^+ and σ^- amplitudes in the cavity even though the driving laser is linearly polarized with equal (symmetric) amplitudes of σ^+ and σ^-.

The purpose of this article is to report the experimental part of the investigation of MIPS. The structure is as follows: First, we briefly summarize for atomic systems with a degenerate lower level the types of steady-state optical switching that are relevant to the physical mechanisms underlying MIPS; second, we present the experimental results; finally, we discuss the significance of the work and summarize our findings.

II. BACKGROUND

There is considerable variety in the steady-state, optical behaviors predicted and observed for a laser-driven cavity able to support two polarization modes and containing a gas of atoms with degenerate lower-level structure.

If coherence effects between lower-level substates can be ignored (the case for a $J=\frac{1}{2}$ to $J=\frac{1}{2}$ transition in zero magnetic field in the simplest excitation geometry), competitive interaction between the modes can be mediated via the atoms through the mechanism of longitudinal optical pumping. The result is that the ratio of σ^+ and σ^- amplitudes in the cavity need not be the same as for the driving laser field. Discontinuous changes in the cavity ratio of σ^+ and σ^- lead to optical tristability[3] and, more generally, polarization switching.[4,5] Experimental observations of these effects have been reported[6-10] for the D_1 line of atomic sodium. In fact, lower-level Zeeman coherences certainly cannot be ignored when the effect of a transverse magnetic field is considered.[8] Coherence generated between ground-state hyperfine levels can also give rise to observable phenomena.[11] In addition, more complex switchings arising from competition between hyperfine and Zeeman pumping have been observed.[9]

It is well known that lower-level coherences can lead to "nonabsorption" resonances,[12] which can be studied by their modification[13] in a magnetic field. The effect of the field is to cause the off-diagonal elements of the density matrix between the lower states to evolve secularly at the Larmor and multiples of the Larmor frequency.[14]

Theoretical consideration of a cavity containing a three-level lambda system allowing such coherence has been shown to give rise to novel schemes for optical bistability[15] and optical multistability,[16] arising principally as a

result of competition between laser-induced creation and Larmor modification or collisional destruction of such coherence. Direct observation of such effects in a three-level lambda system free from complications of other levels has not to our knowledge been reported, although the model can be approximately realized by the Na D_1 transition under appropriate geometrical and buffer-gas conditions.[8,17,18]

III. MOTIVATION

It is desirable that experimental investigation in an optical cavity of the switching behavior for a gas of atoms with lower-level degeneracy should utilize the simplest well-defined suitable transition. To study intrinsic, laser-induced, lower-level coherence effects (as well as longitudinal-optical pumping effects), the simplest choice of atomic transition is $J(\text{lower})=1$ to $J'(\text{upper})=0$.[19]

It is not particularly easy to find suitable atoms with this transition within the tuning range of a continuous-wave Rhodamine-6G dye laser (preferred in order to facilitate reaching the required continuous-wave optical power). We have considered, but discarded, the idea of using transitions between excited states, such as the 585.2-nm $J=1$ to $J'=0$ $1s_2$-$2p_1$ (Paschen notation) transition in Ne I. The crucial disadvantage of this case in neon is the rapid depolarization of the lower $J=1$ level by radiatively trapped spontaneous decay to the true ground state.[20] Since polarization sensitivity in MIPS depends on competition[2,21] between optical pumping and the establishment of Zeeman coherences, it thus depends on the relaxation rates $\Gamma_1(l)$ and $\Gamma_2(l)$ for orientation and alignment decay[22] in the lower level. These should be considerably smaller than other atomic relaxation rates in order that the full possibility for optical switching be readily accessible.

A suitable case is the $[\text{Xe}]4f^6 6s^2\,{}^7F_1$–$[\text{Xe}]4f^6 6s 6p\,{}^7F_0^o$ 570.68-nm transition in Sm I. Although natural samarium consists of a number of even and odd isotopes [22.6% ^{154}Sm, 26.6% ^{152}Sm, 7.4% ^{150}Sm, 13.9% ^{149}Sm ($I=\frac{7}{2}$), 11.3% ^{148}Sm, 15.1% ^{147}Sm ($I=\frac{7}{2}$), and 3.1% ^{144}Sm], the separations of the even ($I=0$) isotope components and hyperfine structure components for this transition are such that it is possible to tune the laser near to an essentially pure $J=1$ to $J'=0$ transition in a single even isotope (Sec. V A 1). This transition has the advantage that an appropriate lower level ($^7F_1$) at 3.63×10^{-2} eV (293 cm^{-1}) is thermally populated from the true ground level, and relaxation within this $J=1$ level is relatively slow at moderate buffer-gas pressure. The disadvantages are the small oscillator strength of the transition (Sec. V A 3) and the high temperature required to produce sufficient atomic absorption for optical switching in cavity.

IV. EXPERIMENT

We have been able[2] to overcome these difficulties by operating with a samarium hollow-cathode discharge lamp[23] inside a near-concentric, Fabry-Perot cavity. The experimental arrangement is shown schematically in Fig. 1. Linearly polarized light from a stabilized continuous-wave dye laser[24] is directed via Faraday isolation, intensity control, and mode-matching optics onto a 256-MHz free-spectral-range, near-concentric Fabry-Perot cavity containing the samarium cell, and is then detected via a Babinet-Soleil compensator, adjusted to quarter wave, and a calcite prism.

A. Samarium cell

Since as far as we are aware the use of a hollow-cathode discharge cell in an optical switching experiment is novel, we describe the procedure used in some detail. The cell is illustrated in Fig. 2.

The temperature required ($\simeq$1000 K) for sufficient samarium vapor pressure to be avaiable to enable an optical switching experiment to be performed in a moderate-finesse Fabry-Perot is not easily compatible with stable interferometer operation. Schlieren effects, in particular, pose a problem, and although the whole oven-interferometer arrangement can be operated in a vacuum, this is inconvenient and to be avoided if possible. A hollow-cathode discharge lamp provides a solution. The basic properties of hollow-cathode lamps and cells for spectroscopy are well known[23] and will not be recounted here. In summary, it has been established that sputtering, and also thermal vaporization if the cathode temperature is sufficiently high, in general lead to controllable densities of atoms, essentially free[25,26] from perturbations due to the discharge. In the case of the weak samarium transition (Sec. V A 3), operation of the hollow-cathode discharge in a pure sputtering mode did not achieve sufficient density of atoms for optical switching. However, by increasing the discharge power to approximately 16 W and allowing the small-bore Sm hollow cathode (typically 3–4 mm internal diameter and 8 mm long) to reach a sufficiently high temperature ($\simeq$1000 K), we could produce an adequate density of samarium. Under these conditions, the discharge was close to unstable (even though current controlled); changes to "glow" or "arc" discharge external to the hollow cathode occurred after approximately 1 h of operation, and resulted in a significant change in discharge voltage (and hence power). Following such a change the cathode usually required replacement.

The buffer-gas (argon) pressure also proved to be important. At too low a pressure (below $\simeq$100 Pa) the

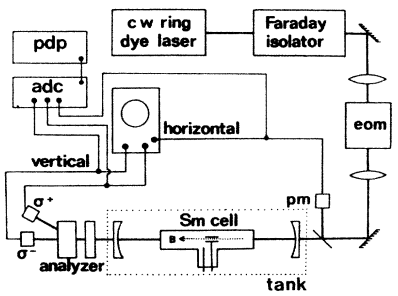

FIG. 1. Experimental arrangement for optical switching studies. The tank (dotted) magnetically shields the optical cavity plus Sm cell; eom, electro-optical modulator; pm, photomultiplier; adc, analog-to-digital converter; pdp-11-03, micro-minicomputer for writing digital data to floppy disk.

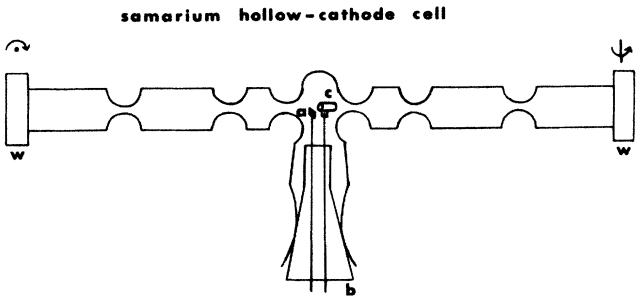

FIG. 2. Samarium hollow-cathode cell. The zirconium anode (a) and the samarium cathode (c), enclosed by a $\simeq$0.15 mm Zr foil, are mounted on tungsten pins in the black-wax sealed demountable base (b). The 1-cm-thick windows (w) are antireflection coated silica flats ($\lambda/10$) inclined ($\simeq 4°$) as indicated. The constrictions in the $\simeq$30-cm-long and 3-cm-diam sidearms of the Pyrex cell help prevent Sm vapor from coating the windows.

discharge failed to enter the hollow cathode and the available voltage (more than 1 kV) did not create sufficient current, and hence discharge power. At too high a pressure (more than $\simeq$300 Pa) the discharge contracted to preferred spots on the inner walls of the cathode, producing an arc, and the voltage required dropped to a value too low to generate sufficient thermal power at maximum current. Accordingly, we applied an intermediate buffer-gas pressure (200$\pm$20 Pa) in the experiments. The length and geometry of the cell and buffer-gas pressure used prevented window contamination by deposited samarium vapor. These 1-cm-thick windows were inclined at a few degrees from normal to the laser-propagation direction to prevent étalon effects, and were antireflection coated on both surfaces (single-pass transmission loss 5%).

The finesse of the cavity plus cell was 27 at zero samarium density. The single-pass power gain was 1.3, and the corresponding total maximum single-pass power at the Sm vapor was $\simeq$160 mW (determined from the measured total output power and the transmissivity of the output mirror which was 0.012). The beam-waist radius at $1/e^2$ intensity was inferred[27] from the spacing of off-axis modes to be 100$\pm$10 μm. Hence, the available maximum cavity intensity (sum of propagating and counter-propagating beam intensities) at the center of the Fabry-Perot amounts to approximately 10^7 W m^{-2} adopting the constant field approximation used in Ref. 28.

B. Conduct of the experiments

The initial experiments were performed by recording σ^+ and σ^- output powers (rather than intensities) on a storage oscilloscope. These experiments were carried out in two modes:

(i) sweeping the laser frequency at constant laser power;

(ii) varying laser power at constant laser frequency.

To ensure linearity of the input-output traces and independence from small beam-steering effects, the detectors[29] were operated well below saturation and were used with integrating spheres. A detector was also used to pick-off from the input beam to supply the horizontal oscilloscope input.

The amount of information that could be recorded in this way under stable conditions was limited. Accordingly, two-channel digitized data were also written to a floppy disk. The digitizing rate per pair of data points (one for each channel) was (64 μs)$^{-1}$ and in a laser-frequency or laser-intensity sweep lasting approximately 0.6 s, 10^4 two-channel (σ^+ and σ^-) data points were accumulated. During this time the critical parameters of the experiment (particularly Sm density and cavity mistuning) remained essentially constant.

In addition to the experiment types (i) and (ii) above, a further experiment was digitally recorded:

(iii) The longitudinal magnetic field was varied sinusoidally with a frequency of 2 Hz while the input power was driven in up-down scans at 40 Hz. This third type of experiment was useful to overcome problems of drift in experimental parameters while the effects of varying the magnetic field were being investigated.

Limitations on data-collection rate in modes (ii) and (iii) meant that only two of the three channels, σ^+, σ^-, and input power could be simultaneously digitially recorded. Plots of both σ^+ and σ^- powers against input power can be inferred from separate scans recording σ^+ against input and σ^- against input. However, such plots are not precisely reproducible because of the effects of laser- and cavity-frequency jitter from run to run. In practice, it proved better to set up the electro-optic modulation circuitry so that nonlinearity in the scan of input intensity versus time was minimized, and record digitally only the σ^+ and σ^- powers. This nonlinearity was less than 2% after the first 25% of scan; the input power axis in Fig. 11 has been drawn to explicitly show the initial nonlinearity.

Type-(ii) constant-frequency experiments provided the most direct observation of optical switching, and a preliminary account of these has already been given.[2] However, these type-(ii) experiments had the disadvantage of providing poor knowledge of the laser-cavity mistuning, and relatively poor resetability in mistuning from run to run. To an extent the type-(i) experiments alleviate this problem by presenting the variation of cavity output with laser frequency. Changes in mistuning with laser frequency are known, and although the absolute mistuning is still uncertain, this uncertainty corresponds to a translation of curves along the frequency axis with the form of the curves largely unaffected by small translations. However, if more than small translations are involved (and the results in Sec. V show that a shift by one free spectral range is enough), the consequent change in laser-atom detuning must also be considered. There is some problem in doing so quantitatively, since the model of a single, homogeneously broadened component is not exact (due to the presence of more than one Doppler-broadened isotope) and, moreover, varies in precision as the laser-atom detuning is changed. We have not attempted to calculate the effect of this in detail. Therefore, the main use to which we put the frequency-scanning results are to indicate the nature of the switching that occurs and to help in understanding the underlying physics.

This leaves the magnetic-field-scanning experiments for comparison with theory. The problem of uncertainty in the *knowledge* of laser-cavity mistuning remains, but the

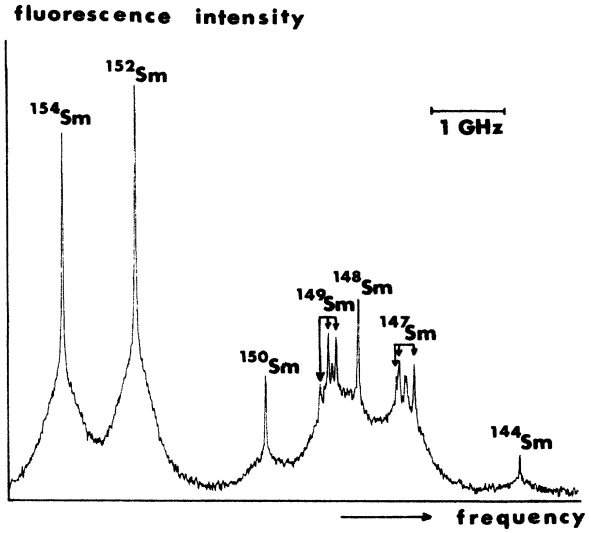

FIG. 3. Doppler-free intermodulated fluorescence spectroscopy scan of the isotope and hyperfine structure of the 570.68-nm Sm I line recorded in a hollow-cathode discharge. Ar buffer-gas pressure 100 Pa. The unlabeled peaks are crossover signals for odd isotopes.

mistuning itself is constant over the regime of the two independent variables, intensity and magnetic field. It therefore seems reasonable to see best-fit agreement to the experimental data by the theory, employing the value of the mistuning as a fitting parameter. This is done in Sec. VI.

C. Subsidiary experiments

As well as the experiments described above, subsidiary experiments were carried out[30] to verify the isotope[31] and hyperfine structure[32] and to establish values of atomic parameters characterizing the Sm $^7F_1$-$^7F_0^o$ 570.68-nm transition. Knowledge of the atomic parameters is important for comparison of experimental with theoretical[33] results.

V. EXPERIMENTAL RESULTS

This section is divided into four subsections. First, results from the subsidiary experiments[30] in the samarium $^7F_1$-$^7F_0^o$ 570.68-nm transition are reported. Second, we give an overview of the observed optical switching behavior using the type-(i) frequency-scanning mode. Third, we present details of selected mode-(i) experimental data and we choose an appropriate cavity-transmission profile to investigate mode-(ii), intensity-scanning results. Finally, we report the mode-(iii) magnetic-field-scanning observations.

A. Subsidiary experiments on Sm $^7F_1$-$^7F_0^o$ 570.68-nm transition

1. Isotope and hyperfine structure

Figure 3 shows a high-resolution scan of the Sm 570.68-nm line recorded by Doppler-free intermodulated fluorescence spectroscopy in a hollow-cathode discharge.[26] The positions of the components are consistent with reported isotope shifts[31] and hyperfine structure.[32] It is interesting to note that the isotope shifts for the 570.68-nm transition, as for other $4f^6 6s^2$-$4f^6 6s 6p$ transitions of Sm,[34] are negative, and hence the observed characteristic spectrum allows this transition to be distinguished from the nearby 570.62- and 570.73-nm transitions, both of which have positive shifts.

2. Samarium temperature and density measurement

Estimates of the temperature of the samarium vapor within the hollow-cathode discharge were made by comparing (Fig. 4) the observed Doppler-broadened absorption profile for the 570.68-nm transition with profiles computed from the known isotope and hyperfine structure. According to saturation vapor pressure data,[35] the deduced temperature of 1000 K would produce a total Sm-atom density of approximately 7×10^{19} m^{-3}. This is to be compared with the value of 12×10^{19} m^{-3} obtained from low-power absorption measurements assuming an oscillator strength of 0.0048 (Sec. V A 3), a thermal population factor of 0.34 for the lower ($^7F_1$) level at 3.63×10^{-2} eV (293 cm^{-1}), and an effective absorption length of 15 mm.

3. Upper-level decay rate

The radiative lifetime of the upper ($^7F_0^o$) level was determined from time-resolved laser-induced fluorescence measurements to be 342 ± 10 ns.[36] With the branching ratio of the 570.68-nm transition taken to be unity, this radiative lifetime yields a value of $f=0.0048$ for the oscillator strength.

The total upper-level decay rate, including depopulation effects of Ar buffer-gas collisions, was found to increase with Ar pressure according to

$$\Gamma_0(u)=[2.9+2.4\times10^{-2}p(\text{Pa})]\times10^6\ \text{s}^{-1}\ ,$$

at a vapor temperature of $\simeq$400 K. Thus for an argon pressure of 200 Pa and vapor temperature of 1000 K,

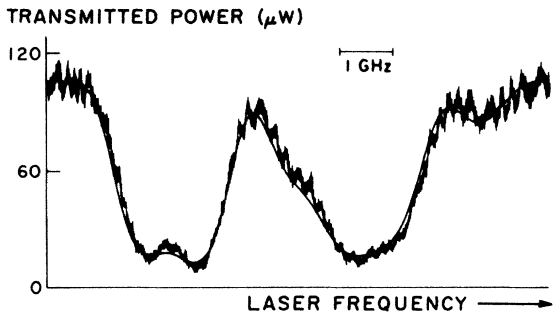

FIG. 4. Doppler-broadened frequency transmission profiles of the 570.68-nm Sm I line. The experimental profile (noisy curve) was obtained from the hollow-cathode cell operated under the same discharge conditions as for the switching experiments, and with a laser power of 110 μW (unfocused beam diameter $\simeq$1.2 mm). The computed profile (smooth curve) is based upon the isotope and hyperfine structure (Fig. 3), assuming a vapor temperature of 1000 K and adjusting for the value of the optical depth.

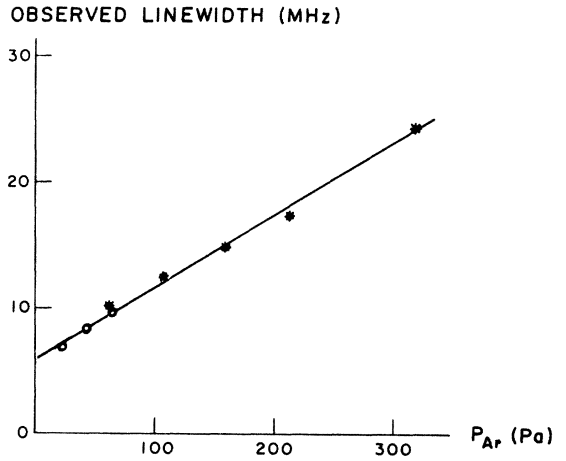

FIG. 5. Observed full width at half maximum for the ^{152}Sm component of intermodulated-fluorescence spectra as a function of buffer-gas pressure at a vapor temperature of approximately 500 K. Hollow-cathode discharge (*); glow discharge (planar cathode) (○).

$\Gamma_0(u)$ is 5.4×10^6 s^{-1}, assuming a $T^{-0.7}$ van der Waals—type temperature dependence for the collisional term.

4. Optical-dipole dephasing rate

The optical-dipole dephasing rate $\Gamma_1(lu)$ for the 570.68-nm transition was determined from the measured pressure dependence of the width of the most intense, ^{152}Sm, component of intermodulated fluorescence spectra, obtained at low laser intensity[26] (Fig. 5). The width at the zero-pressure intercept (6 MHz) originates from a combination of natural broadening (0.47 MHz), laser-bandwidth broadening ($\simeq$2 MHz), residual saturation broadening (1—2 MHz), residual Doppler broadening due to imperfect collinearity of the laser beams ($\simeq$0.5 MHz), and unresolved Zeeman splitting due to stray magnetic fields ($\simeq$0.5 MHz). In particular, it can be shown by comparing spectra taken in a hollow-cathode discharge and a cell with thermally produced vapor that the discharge itself does not contribute significantly to the observed linewidths. Thus the actual homogeneous linewidth (full width at half maximum) at $\simeq$500 K is given by

$$[0.47+5.7\times10^{-2}p(\text{Pa})]\ \text{MHz}\ ,$$

and hence the optical-dipole dephasing rate amounts to $\Gamma_1(lu)=2.4\times10^7$ s^{-1} at 200 Pa and $\simeq$1000 K (assuming a $T^{-0.7}$ temperature dependence for the collisional term).

5. Lower-level depolarization rates

The contribution of argon collisions to the alignment-destruction rate $\Gamma_2(l)$ of the lower ($^7F_1$) level was determined from measurements of the decay of lower-level quantum beats as a function of argon pressure.[25] The method used to detect the lower-level beats was similar to that reported by Mlynek and Lange.[37] Briefly, it consists of using a sharp intense pulse from a nitrogen-laser-pumped dye laser to induce a transient coherence between Zeeman-split $m=\pm1$ states in the lower level and a weak continuous-wave probe beam to monitor transients in the transmission through crossed polarizers. The value of $\Gamma_2(l)$ for argon collisions was found to be 1.1×10^4p(Pa) s^{-1} at $\simeq$600 K, or 1.3×10^6 s^{-1} at 200 Pa Ar and 1000 K (assuming a $T^{-0.7}$ temperature dependence).

Two other effects modify this rate in the conditions of the optical bistability and polarization-switching experiments. The transit time[38] of Sm atoms in the $\simeq$200-μm-diam beam waist in the cavity is approximately 1.2 μs, using a value for the mean free path of 150 μm at 200 Pa argon buffer gas and a temperature of 1000 K. This acts to increase the alignment-destruction rate to the total estimated value of $\Gamma_2(l)=2.1\times10^6$ s^{-1}. However, spin-polarized atoms leaving the region of the beam create a "reservoir" which partially offsets the transit-time effect. This latter effect has not been incorporated into the total value for the alignment-destruction rate $\Gamma_2(l)$.

The orientation-destruction rate $\Gamma_1(l)$ in the lower level also enters into the atomic behavior. Isotropic collisions cause this rate *not* to differ significantly[39,40] from the alignment-destruction rate $\Gamma_2(l)$. Furthermore, transit-time broadening equally affects $\Gamma_1(l)$ and $\Gamma_2(l)$. The fact that the ratio of these two rates is approximately unity $[\Gamma_1(l)\simeq\Gamma_2(l)]$ has important implications regarding the mutual influence of the physical mechanisms acting (see Sec. VI) in the following experiments.

B. Overview of switching behavior

Figures 6 and 7 show plots of the power transmitted by the cavity as the laser frequency is scanned [mode (i)] across the ^{154}Sm and ^{152}Sm components of the 570.68-nm line. As discussed in Secs. III and V A 1, these components are reasonably well separated from the remaining hyperfine structure; their positions, near 1.25 and 2.25 GHz, respectively (the frequency origin has been chosen arbitrarily), show up most clearly in Fig. 6 (zero magnetic field) as the places where there is a local *increase* in Fabry-Perot peak height. This effect, arising from saturated absorption in the bidirectional cavity, is, of course, sensitive to the degree of power broadening, which at approximately 100 MHz for transmission maxima (see the Appendix) is less than both the inhomogeneous width and the cavity free-spectral range.

However, the most significant feature of Fig. 6 is that only simple OB and not PS is observed. The transmitted σ^+ and σ^- powers are equal to each other within measurement error. The situation thus contrasts with similar studies in sodium, where PS is observed (in zero field) for a cavity able to support polarization-degenerate modes,[6,7] and where a polarization-nondegenerate cavity (e.g., possessing internal Brewster-angled surfaces[41]) is required to suppress PS in zero magnetic field for linearly polarized driving.

The switching observed in Fig. 6 is predominantly dispersive OB, similar to the dispersive OB switching reported using frequency scanning in sodium vapor[41] (near the upper-frequency limit on the right-hand side of Fig. 6 the first peak of the backward scan, displaying hysteresis, is shown). Absorptive optical switching is less readily

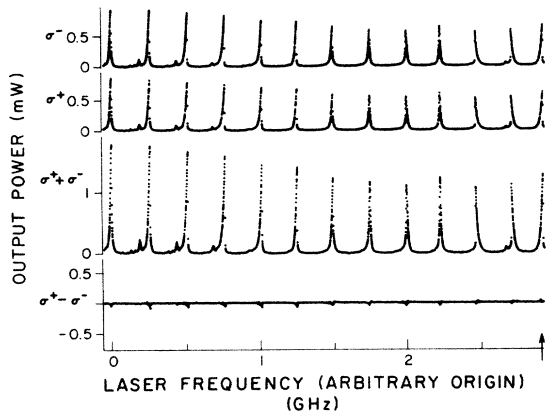

FIG. 6. Circularly polarized powers transmitted by the Fabry-Perot as the laser frequency is scanned [mode (i), increasing frequency] across the ^{154}Sm and ^{152}Sm components (see text) for linearly polarized input power 130 mW and zero magnetic field. The first peak of the backward scan, at the right-hand side of the figure, is indicated by an arrow.

seen (in fact, *not* seen in Fig. 6), owing to the inhibiting effect of inhomogeneous broadening. Such absorptive optical bistability can indeed be observed if both the atom-cavity coupling (i.e., the cooperativity—see Sec. VI) and the cavity power are sufficiently raised. We achieved this in a separate experiment (not reported here) which utilized Brewster-angled windows on the samarium hollow-cathode cell. Because of reduced losses both the cooperativity and the power gain (Sec. IV B) were much higher.

For a longitudinal magnetic field sufficient to produce a Larmor frequency comparable to the lower-level alignment decay rate, the situation is very different. Figure 7 treats the case $B=+168$ μT (the positive sign meaning the field direction is toward the cavity output mirror). Three points are particularly noteworthy. First, the σ^+ and σ^- intensities are no longer equal and PS is occurring over a range of detunings with first one polarization then the other switching "on." This behavior occurs for both directions of frequency sweeps and exhibits hysteresis. (At the arrowed position, near the right-hand side of Fig. 7, we include the start of the backward frequency sweep.) The second point is that the peak absorption at the "center" (meaning the weighted mean position between the ^{154}Sm and ^{152}Sm components) is considerably greater than for zero magnetic field. This is consistent with reduced "black-line" ("nonabsorption" resonance) effects,[12] as will be discussed in Sec. VI. Third, we note that the behavior of σ^+ on the low-frequency side of the ^{154}Sm component (at 0.75 GHz) is similar to the behavior of σ^- on the high-frequency side of the ^{152}Sm component (at 2.5 GHz). This is in accord with the expected symmetry[33] for a $J=1$ to $J'=0$ transition: the behavior of the σ^+ (σ^-) intensity for the laser detuned to the low-frequency side of the transition corresponds to the behavior of the σ^- (σ^+) intensity for the laser equally detuned to the high-frequency side. Figure 7 does not, in fact, reveal this symmetry perfectly, owing to the complexities associated with the existence of *two* principal, not quite equal even-isotope components, as well as other isotope structure. Furthermore, the detunings for the Fabry-Perot transmissions at 0.75 and 2.5 GHz are not evenly spaced from line "center."

C. Detailed switching studies

The above considerations have led us to focus detailed attention on the region of 0.6—1.2 GHz (Figs. 6 and 7), which is well removed from odd-isotope effects, although it is still within the Doppler-broadening region for the ^{154}Sm component. Detunings further removed from line "center" would, in principle, be preferable, in order to improve the approximation of a single, homogeneously broadened $J=1$ to $J'=0$ transition, but to observe interesting switching effects at these increased detunings would entail using increased samarium densities, with the associated experimental problem of very short cell life and difficulty in obtaining consistent sets of data.

Figures 8—10 illustrate, for a range of magnetic fields, expanded frequency scans [mode (i)] in the region 0.6—1.2 GHz. The samarium density ($\sim 10^{20}$ m^{-3}) and laser power (130 mW, linearly polarized) are the same as for Figs. 6 and 7. We note that reversing the direction (sign) of the magnetic field interchanges σ^+ and σ^- outputs (compare Figs. 7 and 9). The mechanism underlying this behavior is discussed in Sec. VI. The expanded frequency scans also reveal the manner in which the Fabry-Perot transmissions are modified as the magnetic field is increased: the profiles for σ^+ and σ^- are shifted further apart in frequency (compare the summed powers $\sigma^+ + \sigma^-$ in Figs. 9 and 10), with (for example) the switching behavior of the profile near to 0.75 GHz in Fig. 10 (-400 μT) being similar to the behavior of the profile with reduced detuning, near 1 GHz, in Fig. 9 (-168 μT).

Further investigation of the switching behavior at $B=-400$ μT has been carried out employing intensity scans at constant laser frequency [mode (ii)]. In particular, the Fabry-Perot profile near 0.75 GHz has been selected as being sufficiently detuned from the ^{154}Sm component to lessen the effects of inhomogeneous broadening, while exhibiting interesting switching behavior. Figure 11 shows the results. The laser intensity has been varied from zero to maximum in 12.5 ms (open circles) and back

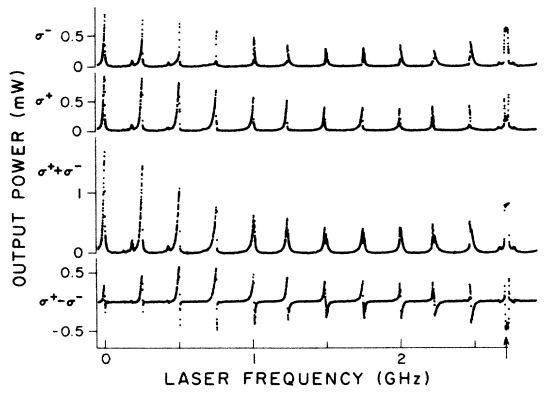

FIG. 7. Circularly polarized powers transmitted by the Fabry-Perot as the laser is scanned [mode (i), increasing frequency] across the ^{154}Sm and ^{152}Sm components for linearly polarized input power 130 mW and $+168$ μT magnetic field. The start of the backward scan is indicated by an arrow.

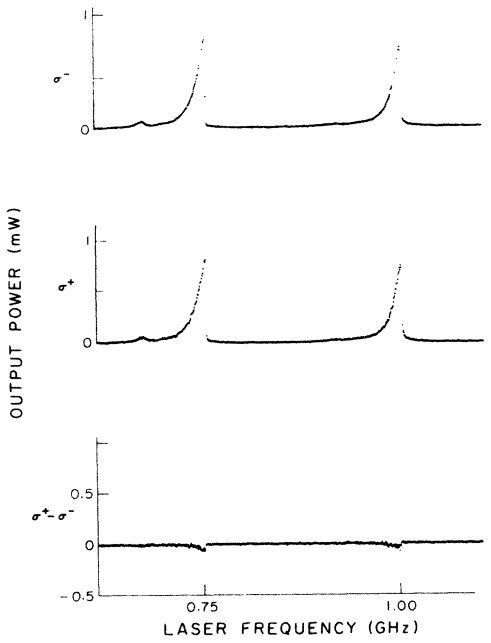

FIG. 8. Expanded frequency scan [mode (i), increasing frequency] at 130 mW input power and zero magnetic field. Upper traces, individual circularly polarized output powers; lower trace, difference power. A small amount of higher-order, off-axis mode structure can be seen.

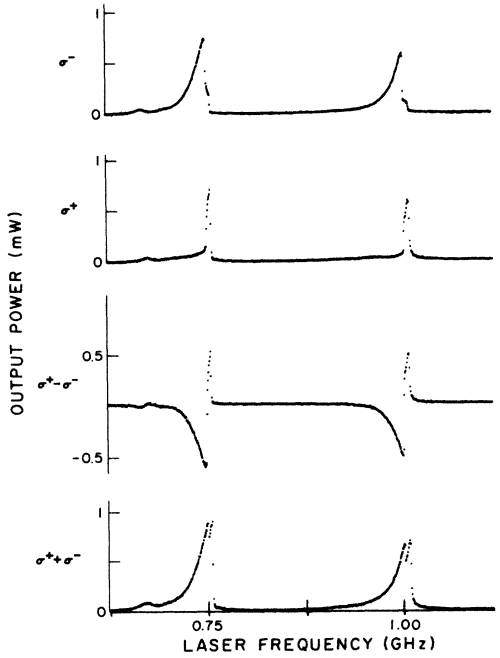

FIG. 9. Expanded frequency scan [mode (i), increasing frequency] at 130 mW input power and -168 μT magnetic field. Upper two traces, individual circularly polarized output powers; lower two traces, difference and sum powers.

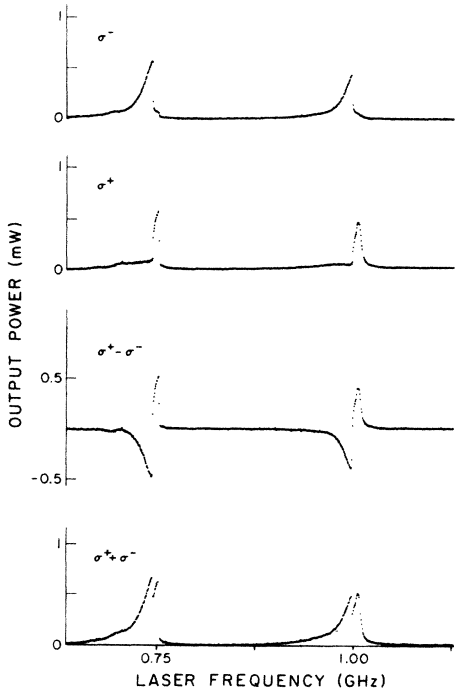

FIG. 10. Expanded frequency scan [mode (i), increasing frequency] at 130 mW input power and magnetic field -400 μT. Upper two traces, individual circularly polarized output powers; lower two traces, difference and sum powers.

to zero in a further 12.5 ms (solid circles). Some hysteresis and definite polarization sensitivity in the switching of σ^+ and σ^- outputs versus input power can be seen in this near-threshold situation [Fig. 11(a)]. When σ^+ and σ^- output powers are plotted against each other [Fig. 11(b)], the polarization character appears more explicitly, although switching and hysteresis are not so obvious, being marked by the distribution of data points along the curve.

D. Magnetic-field-scanning experiment

The remaining effort has been directed to obtain mode-(iii) magnetic-field-scanning results. Figure 12 illustrates the way the data were recorded, σ^- and σ^+ output powers being stored versus time as the input power is periodically (40 Hz) ramped from 0 to 130 mW to 0 [the same as for mode-(ii) results] while the magnetic field is varied sinusoidally (2 Hz frequency, 55 μT amplitude). For convenience, Fig. 12 also displays the difference output power ($\sigma^- - \sigma^+$). Relationships of σ^+ to σ^- powers obtained from the above data are plotted in Fig. 13 for three magnetic field values. As in Fig. 11(b), increasing and decreasing input powers are shown, respectively, as open and solid circles; discontinuities and hystereses in switching appear in terms of the distribution of these.

In Fig. 13(a) the magnetic field is less than 10 μT (compared with the 16 μT needed to give a lower-sublevel separation equal to the alignment-decay rate), and the linear plot confirms symmetry in switching for this case. The remaining, nonlinear plots in Fig. 13 illustrate the pronounced asymmetry between polarizations which develops when the magnetic field (>40 μT) exceeds the

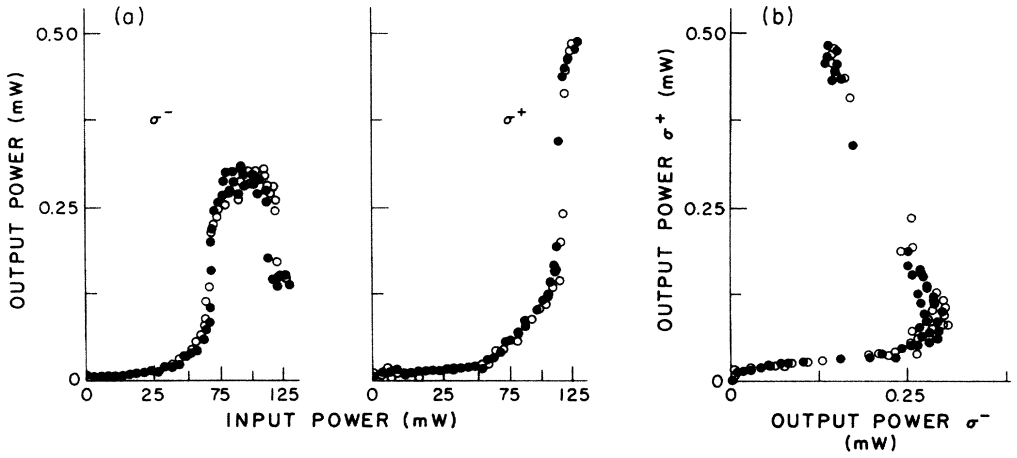

FIG. 11. Up-down intensity scan [mode (ii)] for the Fabry-Perot transmission at $\simeq$0.75 GHz and magnetic field $-400\,\mu$T (see Fig. 10): ○, increasing input intensity; ●, decreasing input intensity. (a) σ^- and σ^+ output powers vs input power; (b) σ^+ vs σ^- output powers. For clarity of presentation, overlapping points have been omitted.

value needed to cause significant Larmor precession in an alignment-relaxation time. Again note that the behavior of σ^+ and σ^- interchanges with reversal of the magnetic field (see Fig. 12).

VI. DISCUSSION

To aid the discussion of the physics of the switchings observed, we recall the expressions given in Ref. 2 (plane-

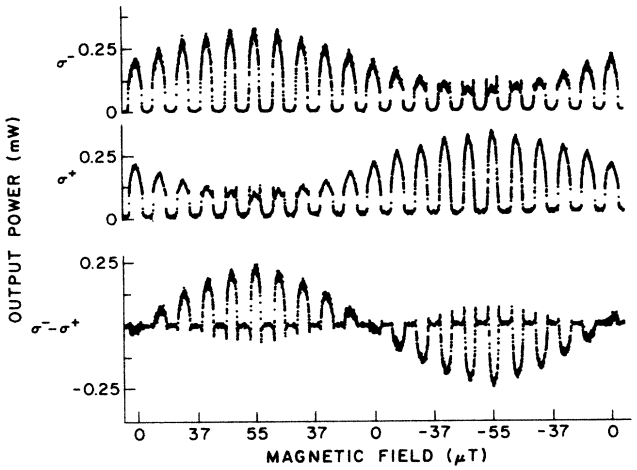

FIG. 12. Sinusoidal magnetic field scan superimposed on up-down power scans [mode (iii)] for the Fabry-Perot transmission at $\simeq$0.75 GHz, and Sm-atom density $\sim 10^{20}\,\mathrm{m}^{-3}$. Upper traces, σ^- and σ^+ output powers; lower trace, difference $(\sigma^- - \sigma^+)$ output power. The σ^+ behavior for positive magnetic field is similar to the σ^- behavior for negative magnetic field, and vice versa. For clarity of presentation overlapping points have been omitted.

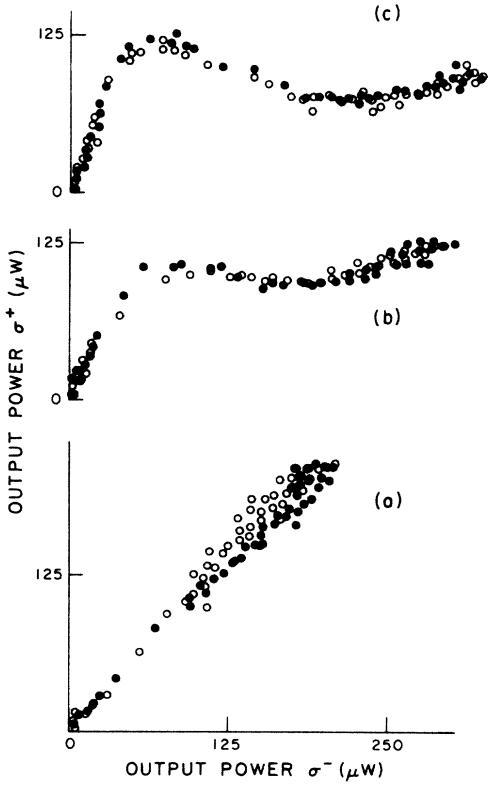

FIG. 13. σ^+ vs σ^- output powers extracted from the data of Fig. 12 for individual up-down scans with the following magnetic field values: (a) 0 μT ($<10\,\mu$T); (b) $45\pm5\,\mu$T; (c) $55\pm5\,\mu$T. Up (○) and down (●) scan data correspond to sightly different values of the magnetic field because of the variation in magnetic field during a single up-down scan. The laser-cavity mistuning is constant, but not precisely determined. For clarity of presentation, overlapping points have been omitted.

wave, ring-cavity, mean-field, homogeneous broadening, $J=1$-$J'=0$ model):

$$Y_{\pm}=X_{\pm}(1+2C\eta_{\pm}-i\phi)\ , \tag{1}$$

relating scaled output fields X_+, X_- to scaled input fields Y_+, Y_- via the cooperativity C (see the Appendix), scaled laser-cavity mistuning ϕ, and coupling functions η_+ and η_-, and

$$\eta_{\pm}=\frac{3}{1-i(\Delta\mp\omega)}\left[[n_{\mp}(l)-n(u)]+\frac{X_{\mp}}{X_{\pm}}\rho^2_{\pm 2}(l)\right]\ , \tag{2}$$

where $n_+(l)$, $n_-(l)$, and $n(u)$ are populations, respectively, of the $J=1$ ($m_J=1$), $J=1$ ($m_J=-1$), and $J'=0$ states and $\rho^2_{+2}(l)$ [$=\rho^{2*}_{-2}(l)$] is the alignment coherence[22] in the lower level. The laser-atom detuning Δ and the Larmor frequency ω are scaled in terms of the optical-dipole dephasing rate $\Gamma_1(lu)$. Further details are included in Ref. 33.

A. $B=0$ case

For $B=0$ and linearly polarized excitation ($Y_+=Y_-$), there is no *a priori* preference between X_+ and X_-; however, the solution $X_+=X_-$ may be stable or unstable. The essential issue is whether a fluctuation-generated imbalance between cavity fields X_+ and X_- will be enhanced or reduced. For sufficient positive feedback, enhancement leads to polarization switching (PS). On the other hand, negative feedback stabilizes the cavity against PS, and simple optical bistability (OB) is observed.

In formal terms, such a fluctuation acts via modification to the susceptibilities for the σ^+,σ^- transitions, that is to say via the coupling functions η_+ and η_-. A difference between these functions arises [Eq. (2)] either from differences between $n_-(l)$ and $n_+(l)$ (longitudinal-optical pumping) or from differing ratios X_-/X_+, X_+/X_- multiplying a nonzero coherence $\rho^2_{+2}(l)$.

The term $X_{\mp}\rho^2_{\pm 2}(l)/X_{\pm}$, which we call the "coherence contribution," is negative,[33] as suggested by the nonabsorption character of its effect on η_+ and η_-. Thus, since (for constant Δ) a change in $n_-(l)$ compared to $n_+(l)$ via longitudinal-optical pumping must imply a change of the same sign in X_-/X_+, the coherence contribution always (for $\omega=0$) acts to *reduce*[42] the effect of changes in the "population contribution," $n_{\mp}(l)-n(u)$, on $\eta_{\pm}$. It is discussed in Refs. 2 and 21 that in the physically realistic case, where $\Gamma_2(l)\simeq\Gamma_1(l)$, the coherence contribution essentially cancels the population contribution to changes in $\eta_+-\eta_-$. Thus, whatever the nature of the feedback from the population contribution (and this depends on the values of Δ and ϕ), the polarization behavior of the system is effectively neutral for zero magnetic field, and polarization switching does not occur for zero field irrespective of laser-atom detuning.

It is helpful to look at this issue in more physical terms. A nonzero $\rho^2_2(l)$ [$=\rho^{2*}_{-2}(l)$] implies that in the lower-level charge distribution there is a nonzero electric quadrupole moment characterizing a nonspherically symmetric distribution of atomic alignment.[22,43] In the limiting case of maximum quadrupole moment (maximum alignment), the linearly polarized cavity field no longer couples population into the upper level (the nonabsorption resonance effect mentioned earlier). In fact, isotropic collisions act to reduce the magnitude of the moment, though they do not change the principal-axis directions of the quadrupole distribution (or strictly speaking, of the alignment ellipsoid), so that coupling to the upper state is not, in practice, reduced to zero.

This coupling can be increased in two ways: either by a change in the polarization state of the cavity field, or by a change in the quadrupole character of the charge distribution, i.e., rotation of the principal-axis directions, or reduction in magnitude of the quadrupole moment.

The former effect underlies the mechanism that inhibits polarization switching for zero magnetic field. In essence, this effect is an *anti*bleaching one, whereas normal population (i.e., longitudinal-) optical pumping, which creates a magnetic dipole oriented parallel (or antiparallel) to the cavity axis, produces *increased* bleaching when the cavity field departs from linearly polarized. Given equality in relaxation rates for the electric-quadrupole and magnetic-dipole moments in the lower state, the bleaching and antibleaching effects cancel. The system behavior is then polarization insensitive.

B. $B\neq 0$ case

A nonzero longitudinal magnetic field increases coupling into the upper state by modifying the coherence $\rho^2_2(l)$, that is, by altering the character of the lower-level quadrupole charge distribution. Larmor precession causes change in principal-axis directions and tends to average the charge distribution toward cylindrical symmetry about the magnetic field direction. It is then no longer the case that change of polarization of the cavity electric field will necessarily give rise to a coherence-based, antibleaching effect. Indeed, a change in the polarization can be found that *enhances* bleaching. For this change in polarization, Zeeman coherence effects and population pumping reinforce rather than cancel each other.

Thus polarization-sensitive behavior becomes possible. The detailed formal dependence of the Zeeman coherence upon competition between cavity-field-induced creation and magnetic-field-induced modification cannot be discussed here. Therefore we are not in a position to explain all the features of the intensity-scanning and magnetic-field-scanning experiments, for which this competition plays a major role.

However, the mode-(i) frequency-scanning experiments carried out at constant laser power can be qualitatively understood largely in terms of the behavior of just the population contributions $n_{\mp}(l)-n(u)$.

1. Small laser-atom detuning

Strictly speaking, there is no region of pure absorptive behavior. However, for zero magnetic field, as in Fig. 6, there is a frequency region around 1.75 GHz between the ^{154}Sm and ^{152}Sm isotopes with reduced nonlinear dispersion where nonlinear absorption dominates. The peak near 1.75 GHz is essentially symmetric in laser-cavity mistuning compared to adjacent peaks, and there is approximate reversal of frequency-pulling effects over the

range 1–2.5 GHz, centered at 1.75 GHz. Indeed, in Sec. V B we noted the similarity of the present switching character with the case of optical bistability in a largely homogeneously broadened transition. It is useful to adopt here a similar approximation of a single-component (though not homogeneously broadened) transition for the purpose of qualitative explanation. This approximation supports the concept of a region of absorptive dominance around the effective line center.

Nevertheless, when a magnetic field is applied, as in Fig. 7, dispersive effects *must* be included. In physical terms, one of the cavity resonances will now, in general, be favored. This can be seen formally from the presence in Eq. (2) of the $\mp\omega$ terms which lead to differing $\eta_{\pm}$ and hence [see Eq. (1)] to differing $X_{\pm}$. Given modification of the Zeeman coherence by the magnetic field as discussed above, the feedback associated with $n_{\mp}(l)-n(u)$ can be enhanced. That this feedback is positive can be easily seen. For example, if X_+ is initially favored, there will be longitudinal optical pumping reducing $n_-(l)$ [and increasing $n_+(l)$], and thus η_+ (η_-) will reduce (increase), and, for constant Y_+ (Y_-), X_+ (X_-) will further increase (reduce). That is to say, polarization-sensitive behavior will, in general, occur.

Experimentally, for $B\neq 0$ the asymmetric shape of the σ^+ and σ^- curves (particularly Fig. 7 at 1.5 and 1.75 GHz) shows that significant nonlinearity is indeed present (compare with Fig. 6 at 1.5 and 1.75 GHz). The polarization of the peak which first becomes pronounced as the laser frequency is increased is the one (σ^+) for which cavity resonance occurs at lower laser frequency. The cavity resonance with opposite polarization (σ^-) is initially suppressed through increased absorption. As the laser frequency is raised further, the saturation reverses (optical pumping changes sign, σ^- pronounced and σ^+ suppressed). The initially suppressed polarization (σ^-) then becomes dominant. The above behavior can be seen in the Fabry-Perot (FP) transmission at 1.5 GHz in Fig. 7. Clearly, when the magnetic field is reversed (ω changes sign) the overall relative dominance between σ^+ and σ^- is also expected to be reversed, as is observed.

If the positive feedback discussed above is sufficiently large, discontinuous switching between σ^+ dominant and σ^- dominant will occur. It appears from Fig. 7 that the critical conditions for such "absorptive PS" are not quite (or perhaps only just) met; the individual Fabry-Perot transmissions for σ^+ and σ^- at $\simeq$1.5 GHz are nearly continuous, whereas there are clear indications of discontinuities for surrounding FP transmissions.

Certainly, absorptive OB is not obvious near 1.75 GHz (Fig. 6), while dispersive OB (Fig. 6) and dispersive PS (Fig. 7) are clearly seen around (for example) 0.75 GHz.

2. *Significant laser-atom detuning*

Most of the detailed emphasis in this investigation has been on switchings seen for laser detunings from the ^{154}Sm isotope of around -500 MHz (at 0.75 GHz in Figs. 6 and 7). In this region, which is within the Doppler broadening associated with the ^{154}Sm transition, both nonlinear absorptive and nonlinear dispersive effects contribute. The latter effects act quite differently from the former. The dominant dispersive nonlinear effect is to tilt the axis of the analytic FP transmissions away from vertical.[28] For the negative laser-atom detuning case shown in detail in Figs. 8 and 9, the greater-than-unity refractive index of the vapor displaces "dressed" FP transmissions to lower laser frequency compared to the "undressed" (zero-vapor) case. At high cavity intensity, through saturation, the dressed transmission frequency returns nearer to the undressed value. For $B=0$ (Fig. 8), simple, largely dispersive OB appears. However, for $B\neq 0$ (Fig. 9) polarization asymmetric behavior is observed.

Within the vicinity of a given transmission peak we distinguish three regions in dispersion-based switchings. First, as the laser frequency moves from a low value toward the dressed transmission, negative feedback stabilizes the cavity output: an increase in cavity field causes movement of the associated transmission toward higher frequency, which reduces the fluctuation. Even though the two polarizations σ^+ and σ^- will now not be degenerate, the dispersive negative feedback tends to constrain the two polarization intensities toward equality. This is markedly different in effect from the absorptive case, when imbalance between polarizations is enhanced. In fact, as can be seen in Fig. 9, neither absorptive or dispersive mechanisms totally dominate in this region. However, the balance shifts toward absorptive dominance for increased laser frequency (see also Fig. 7).

In the next region, as the laser frequency moves past the peak of the pulled, dressed more dominant (σ^- for $B<0$) transmission, the feedback for this polarization changes sign. A reduction in this polarization will be reinforced, and accompanied by an increase in the initially less dominant polarization. In this region the order of dominance becomes strongly reversed (σ^+ intensity $\gg\sigma^-$ intensity).

The final region is characterized by the limit being reached on frequency pulling for the now dominant (σ^+) polarization so that this polarization also decreases sharply. In the cases shown (Fig. 9) discontinuous changes are seen. Again, it is clear that the overall behavior between σ^+ and σ^- is expected to reverse with reversal in direction of the magnetic field.

For the transmission at lower frequency in Fig. 9 (0.75 GHz) the explanation above suffices reasonably well. However, additional switching to an intermediate transmitting state on the steep portion of the curve does occur and is even more pronounced for the transmission at higher frequency (1.0 GHz). Not only are absorptive effects more important, but coherence effects also play a significant role, and the intermediate transmitting state appears to have similar (though not identical) features to "coherence-based" OB.[15] On increase of the magnetic field (Fig. 10) similar arguments apply, but we note that it is even more difficult to demarcate absorptive, dispersive, and coherence effects.

C. Analysis of the magnetic-field-sweeping results

1. *Comparison of theoretical and experimental results*

Although we shall not attempt here detailed explanations of the way these absorptive, dispersive, and coher-

ence effects interrelate,[33] it is worthwhile to show—by comparison of the results in Sec. V D with the theory—that the observed phenomenology is displayed by the $J=1\text{-}J'=0$ mean-field plane-wave, ring-cavity, homogeneous-broadening model.

Figures 14 and 15 illustrate model up-down intensity scans corresponding to magnetic field values 0, 37 and 55 μT, labeled in Fig. 12. In Fig. 14, σ^- and σ^+ output intensities and the difference intensity $\sigma^-\text{-}\sigma^+$ are plotted (cf. Fig. 12), while Fig. 15 shows the relationships of σ^+ to σ^- intensities (cf. Fig. 13). Many of the experimental features are quite well represented in the theory. In particular, the reversal in dominance between polarizations with increasing input power near to maximum field (55 μT) is clearly predicted. The experiment does, however, show growth of the less dominant polarization with input power (near maximum magnetic field), in contrast to theoretical prediction. This may be due to saturation of inhomogeneous-broadening-based absorption. It is interesting to note the changeover which occurs from discontinuous switching behavior at low field to continuous behavior at maximum field. This derives from magnetic field modification to the nonabsorption resonance influence [via $\rho_2^2(l)$] on the "dressed" cavity phase shifts (described in terms of the imaginary parts of η_+ and η_-).

2. *Discussion of model parameter values*

Strictly speaking, the plane-wave, ring-cavity, homogeneous-broadening model cannot be expected to apply to an experiment involving a standing-wave cavity with Gaussian-spatial-mode structure and an inhomogeneously broadened transition. Particularly, there is no unique way, in general, to relate[41] the actual distribution of cavity electric field intensities to the single value characterizing the mean-field plane-wave intensity. Nevertheless, for a restricted range of parameters, an effective identification may be possible. Our present concern is to look at this issue of an appropriate scaling for the (restricted) conditions applying to the magnetic-field-scanning data.

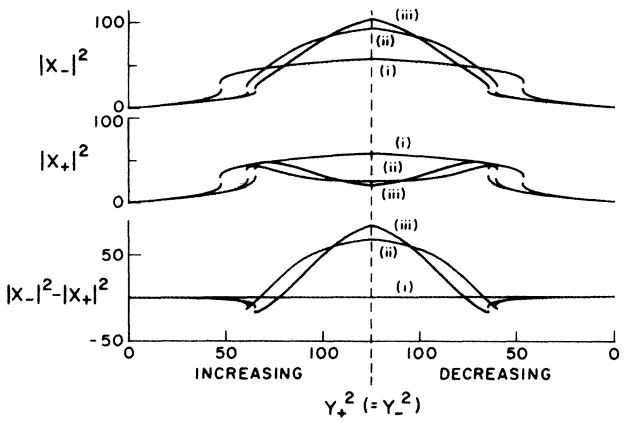

FIG. 14. Theoretical output intensities modeling experimental up-down scans for the following magnetic fields: (i) 0 μT ($\omega=0$); (ii) 37 μT ($\omega=0.2$); (iii) 55 μT ($\omega=0.3$) (cf. Fig. 12 and see text). Cooperativity (C), 2000; laser-atom detuning, -150; radiative decay rate, 0.25; and lower-state relaxation rates [$\Gamma_1(l)=\Gamma_2(l)$], 0.0875, in units of the homogeneous half-width half-maximum for the transition; laser-cavity mistuning, -24.5, in units of the cavity half-width half-maximum.

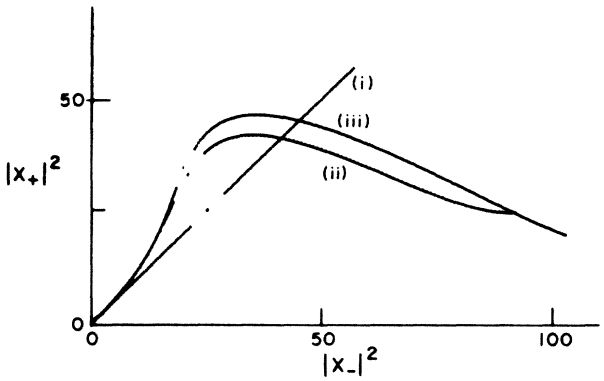

FIG. 15. Theoretical σ^+ vs σ^- output intensities for values of magnetic field corresponding to those in Fig. 14: (i) 0 μT; (ii) 37 μT; (iii) 55 μT. Other parameters are the same as for Fig. 14.

If these data had been recorded entirely in the dispersive regime, then we might argue by analogy with the homogeneous-broadening Gaussian-mode OB case[44] that we should be able to apply the model, utilizing an effective averaged intensity of 75% of the actual averaged on-axis Fabry-Perot intensity. In fact, absorptive effects are important, as we can see from the value of the laser detuning, within the Doppler profile of the ^{154}Sm isotope. Arguing from the experience with OB results, where it is known that Doppler broadening and Gaussian-mode structure both lead to substantial raising of threshold cooperativity and incident power for the observation of absorptive critical-point switching, we suspect a similar substantial raising of threshold conditions would apply for critical switching in the present case.

As a rough estimate of the size of these effects, we note that the threshold input power scales as Δ^3/C in the dispersive OB case.[44] An increase in Δ by a factor of between 2 and 3 would (see Fig. 4) take us into the Lorentzian tail of the atomic absorption, and hence would allow a homogeneous model to be applied. This should result in at least an order of magnitude increase in predicted threshold power. However, experimentally, the observation of switchings at these increased detunings requires very modest, if any, power increase. Thus we expect that the experimental intensity for critical switching in the magnetic-field-sweeping data should be at least an order of magnitude greater than the value giving a good fit for the model.

A further factor of about 3 discrepancy between predicted and observed intensities is introduced by the value of C used. The theoretical plots of Figs. 14 and 15

are based upon $C=2000$, whereas the value of C obtained from the procedure in the Appendix (for a total Sm density of 1.2×10^{20} m^{-3}) is 560 for ^{154}Sm alone or about 600 if the ^{152}Sm-isotope contribution is included, but the ^{154}Sm value of Δ is retained for application of the theory. The basis for this figure is the result that for a mixture of even isotopes, each homogeneously broadened and described by the same parameters except for detuning and concentration, the separate values of C/Δ^3 are simply added for the dispersive regime.

Thus, overall, we expect the experimentally observed intensity to be $1\frac{1}{2}$–2 orders of magnitude larger than the fitted theoretical value. In fact (using the Appendix), we obtain experimentally that Y^2 should be 3200 (on axis) or 2400 (averaged over the Gaussian mode), compared with a fitted value for the model of 250. Thus the discrepancy appears to be nearer to 1 order of magnitude. The arguments above are, of course, very approximate. Regarding the parameters other than intensity used for the model, Δ has been chosen appropriately for the ^{154}Sm isotope, since this isotope has the major influence on the magnetic scanning results. The value $C=2000$ is somewhat heuristic; the use of a value larger than predicted for the homogeneous-broadening model probably helps adjust for neglect of inhomogeneous broadening by increasing the importance of absorptive effects. Finally, as explained earlier, the laser-cavity mistuning has been fitted since its precise value is not known. However, the value of -24.5 times the empty-cavity half-width at half-height is consistent with the amount of cavity pulling observed as the Sm density was raised.

In view of the considerable complexity of the $J=1$ to $J'=0$ polarization-switching theory even in the mean-field, plane-wave, ring-cavity case, and the lack of detailed knowledge of some of the critical experimental parameters, we have not attempted a more complete quantitative comparison. Among other effects, it is clear that to obtain valid quantitative comparison of theoretical with experimental switching thresholds, the cavity used must be modeled realistically.[45,46] However, we believe we have established in qualitative terms that the phenomenology of the switching observed in this $J=1$-$J'=0$ experiment is in accord with the behavior predicted for the $J=1$-$J'=0$ model.

VII. SUMMARY

We have experimentally investigated the steady-state nonlinear behavior of the $4f^6 6s^2\,{}^7F_1$ to $4f^6 6s 6p\,{}^7F_0^o$ 570.68-nm transition of Sm I in a Fabry-Perot cavity driven near resonantly by linearly polarized continuous-wave laser excitation. In zero magnetic field we find that the symmetry in polarization (equal intensities of σ^+ and σ^-) is conserved in the transmission by the Fabry-Perot. The balancing effects of longitudinal-optical pumping and laser-induced lower-level coherence cause the $J_{\text{lower}}=1$ to $J_{\text{upper}}=0$ transition in zero field to behave effectively as a two-state transition showing only simple optical bistability with no polarization sensitivity in switching. However, upon application of a steady longitudinal magnetic field sufficient to produce a lower-level Larmor frequency comparable to the lower-level alignment-decay rate, we find that polarization differences are developed in the cavity output.

For sufficient laser power in the optical cavity and sufficient samarium density, polarization-sensitive switchings occur, with lowest-power threshold occurring at nonzero laser-atom detuning for this inhomogeneously broadened situation. The behavior of the two (σ^+ and σ^-) polarizations interchanges upon reversal of the orientation of the magnetic field, as expected from the symmetry of the transition. Effects of both nonlinear absorption and nonlinear dispersion are seen. The feedbacks from these act quite differently in determining the polarization behavior in a nonzero magnetic field. The detailed character of the switching is thus highly sensitive to laser-atom detuning.

The phenomenology of the switching can be understood in terms of the model of $J_{\text{lower}}=1$ to $J_{\text{upper}}=0$ atoms in a plane-wave ring cavity.

ACKNOWLEDGMENTS

We gratefully acknowledge valuable assistance from Dr. R. J. Ballagh, Professor J. N. Dodd, and Mr. D. S. Gough. Particularly, we thank Rob Ballagh warmly for helping us firm up our ideas and for a careful reading of the manuscript. One of us (P.H.) wishes to acknowledge support from the Willian Evans Visiting Fellow Program. A substantial part of the experimental apparatus construction was previously undertaken by Dr. M. W. Hamilton and Dr. D. M. Warrington, and Mr. J. S. Satchell. We have also benefited from the willing support of Messrs. R. Gledhill, R. Mewhinney, and W. Hastie, and other University of Otago technical staff. Another of us (W.J.S.) wishes to thank Dr. J. Cooper and Dr. A. Gallagher for helpful comments during preparation of the manuscript. He also wishes to gratefully acknowledge both the support of the JILA Visiting Fellow Program the prior support of the Max-Planck-Institut für Quantenoptik, Garching, Federal Republic of Germany. Finally, we acknowledge financial support from the New Zealand Universities Grants Committee and the Research Committee of the University of Otago.

APPENDIX

In obtaining an expression for the saturation behavior of the Sm 570.68-nm transition, we adopt the picture illustrated in Fig. 16. The upper-state total decay rate $\Gamma_0(u)$ differs from the radiative value γ_u; we take account of this by assuming collisional coupling of the $J=0$ upper state u to a separate (assumed nondegenerate) state u'. Similarly the $J=1$ lower state l is assumed collisionally coupled to the $J=0$ true ground state l'. Radiative decay connects u only with l (rate γ_u) and (we suppose) u' only with l' (rate $\gamma_{u'}$).

For the solution of the full problem, transitions σ^+ and σ^- may be driven at differing rates by (respectively) fields X_+ and X_-. Since this solution is prohibitively lengthy, we consider only the more simple, linearly polarized "symmetric" case, $X_+=X_-$, in zero magnetic field. Then it is convenient to consider a rotation of the quanti-

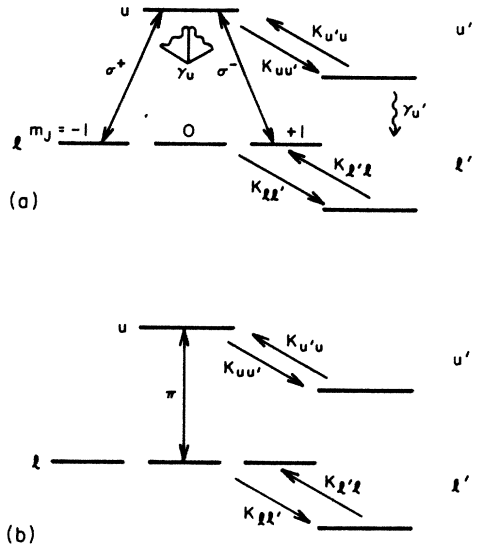

FIG. 16. Atomic energy levels assumed to participate in the saturation behavior of the Sm 570.68-nm transition. (a) Quantization axis taken parallel to laser propagation direction; (b) quantization axis taken parallel to laser electric field direction.

zation axis by $\pi/2$ which converts the linear $\sigma^{\pm}$ excitation [Fig. 16(a)] to linear π [Fig. 16(b)].

Because of the spherical symmetry of both the collision processes and radiative decay, it is appropriate to express the density matrix in terms of irreducible tensor components $\rho_q^k(\alpha\beta)$ for the u, u' l, and l' states. The relevant equations of motion for π-polarized excitation $E\cos(\omega_L t)$ can be written (in the rotating-wave approximation) with inhomogeneous broadening assumed dominated by homogeneous broadening and the time dependence of the electric field removed by transformation to the rotating frame:[47]

$$\dot{\rho}_0^0(u)=-(\gamma_u+K_{uu'})\rho_0^0(u)+K_{u'u}\rho_0^0(u') + \frac{iEd}{2\sqrt{3}\hbar}[\rho_0^1(lu)+\rho_0^1(ul)] , \tag{A1a}$$

$$\dot{\rho}_0^0(u')=-(\gamma_{u'}K_{u'u})\rho_0^0(u')+K_{uu'}\rho_0^0(u) , \tag{A1b}$$

$$\dot{\rho}_0^0(l)=-K_{ll'}\rho_0^0(l)+(K_{l'l}/\sqrt{3})\rho_0^0(l') +(\gamma_u/\sqrt{3})\rho_0^0(u)-\frac{iEd}{6\hbar}[\rho_0^1(lu)+\rho_0^1(ul)] , \tag{A1c}$$

$$\dot{\rho}_0^0(l')=-K_{l'l}\rho_0^0(l')+\sqrt{3}K_{ll'}\rho_0^0(l)+\gamma_{u'}\rho_0^0(u') , \tag{A1d}$$

$$\dot{\rho}_0^2(l)=-\Gamma_2(l)\rho_0^2(l)+\frac{iEd}{3\sqrt{2}\hbar}[\rho_0^1(lu)+\rho_0^1(ul)] , \tag{A1e}$$

$$\dot{\rho}_0^1(lu)=-[i(\omega_L-\omega_{lu})+\Gamma_1(lu)]\rho_0^1(lu) +\frac{iEd}{\hbar}\left[\frac{1}{2\sqrt{3}}\rho_0^0(u)-\tfrac{1}{6}\rho_0^0(l)+\frac{1}{3\sqrt{2}}\rho_0^2(l)\right] . \tag{A1f}$$

In Eqs. (A1), d is the reduced dipole matrix element connecting l and u states. Laser coupling between states l' and u' is ignored. (Factors of $\sqrt{3}$ enter into some of the collisional terms due to normalization.)

In addition, closure requires

$$\sqrt{3}\rho_0^0(l)+\rho_0^0(u)+\rho_0^0(l')+\rho_0^0(u')=1 . \tag{A2}$$

The solution to Eqs. (A1) and (A2) in the steady state is

$$\rho_0^1(ul)=\frac{(\Delta-i)Xf}{1+\Delta^2+bX^2} , \tag{A3}$$

where the scaled field X is

$$X=Ed/[2\sqrt{3}\hbar\Gamma_1(lu)] , \tag{A4}$$

the scaled detuning is

$$\Delta=(\omega_L-\omega_{lu})/\Gamma_1(lu) , \tag{A5}$$

and the coefficients f, b have the form

$$f=1/[3(1+K_{ll'}/K_{l'l})] , \tag{A6a}$$

$$b=\frac{2}{3}\frac{\Gamma_1(lu)}{\gamma_u+K_{uu'}}\frac{1}{1+K_{ll'}/K_{l'l}}\frac{(\gamma_\mu+K_{uu'})(\gamma_{u'}+K_{u'u})}{\gamma_u\gamma_{u'}+\gamma_uK_{u'u}+\gamma_{u'}K_{uu'}} \times\left[4+\frac{K_{uu'}}{K_{l'l}}+3\frac{K_{ll'}}{K_{l'l}}+\frac{\gamma_{\mu'}K_{uu'}}{(\gamma_{u'}+K_{u'u})K_{l'l}}+2\frac{(1+K_{ll'}/K_{l'l})(\gamma_u\gamma_{u'}+\gamma_uK_{u'u}+\gamma_{u'}K_{uu'})}{\Gamma_2(l)(\gamma_{u'}+K_{u'u})}\right] . \tag{A6b}$$

Note the important conclusion that Eq. (A3) has an effective two-state form. In the limit $K_{uu'}=K_{u'u}=K_{ll'}\to 0$, $K_{l'l}\neq 0$, Eq. (A3) reduces to Eq. (9) of Ref. 48, and in the limit $\Gamma_2(l)\to\infty$, Eq. (A3) is consistent (apart from factors arising from differing degeneracy) with the steady-state result of Cooper and Ballagh.[49]

For the calculation of the value of the on-axis saturation field in terms of the single-pass power gain G, the laser power P_L, and the waist radius W_0, we use the expression[41]

$$E=\left[\frac{8GP_L}{\pi W_0^2\varepsilon_0 c}\right]^{1/2} . \tag{A7}$$

The reduced dipole matrix element d is obtained from the radiative rate γ_u:

$$\gamma_u = \frac{\omega_{lu}^3}{3\pi\varepsilon_0\hbar c^3} d^2 . \tag{A8}$$

Values of the rates γ_u, $\Gamma_0(u)$, $\Gamma_1(lu)$, and $\Gamma_2(l)$ are obtained from Sec. V A. The effective collisional rates are estimated as follows:

$$K_{u'u} = K_{uu'} = \Gamma_0(u) - \gamma_u , \tag{A9a}$$

$$K_{ll'} = t^{-1} , \tag{A9b}$$

where t is the beam transit time (Sec. V A 5), and

$$K_{l'l} = K_{ll'} e^{-\varepsilon/k_B T} \tag{A9c}$$

(i.e., detailed balance is assumed with ε being the energy of the state l referred to the true ground state l'). Finally, the decay rate $\gamma_{u'}$ is assumed sufficiently rapid that its value (and therefore also the value of $K_{u'u}$) drops out of Eq. (A6b).

In practical terms, the values of b for the cases of collisional coupling to u' and l', and of no collisional coupling to u' and l', are the same to within a few percent; the effect of this coupling has therefore been ignored in the calculation of the scaled power parameters. This procedure remains valid even if a finite rate, e.g., (157 ns)$^{-1}$,[50] is assumed for $\gamma_{u'}$.

We require three further results. The first is the degree of resonant power broadening for the zero-velocity group (see Sec. V B) averaged over the Gaussian cavity mode. We employ Eqs. (35) and (38) from Ref. 44, and seek the value of the scaled detuning, $\Delta_{1/2}$, for which the power-broadened absorption coefficient

$$\alpha = \frac{2\alpha_0}{X^2} \ln\left\{\frac{1}{2}\left[\left\{\frac{1+\Delta^2+2X^2}{1+\Delta^2}\right\}^{1/2}+1\right]\right\} \tag{A10}$$

falls to half its $\Delta=0$ value. The power-broadened full width at half-height is then twice $\Delta_{1/2}$.

The second result we need is an expression for the low-field absorption coefficient α_0, treating the transition as homogeneously broadened. From

$$\alpha_0 = -\frac{i\omega_{lu}}{c}\chi(\Delta=0) ,$$

where the susceptibility, χ, is given in terms of the total density N of atoms by

$$\chi = -Nd/(\sqrt{3}\varepsilon_0)[\rho_0^1(ul) - \rho_0^1(lu)]/E ,$$

we find

$$\alpha_0 = \frac{\lambda^2}{4\pi}\frac{\gamma_u}{\Gamma_1(lu)} Nf .$$

Substituting for f from Eq. (A6a), this yields

$$\alpha_0 = \tfrac{1}{3} N_l \lambda^2 \gamma_u / [4\pi\Gamma_1(lu)] , \tag{A11}$$

where N_l is a thermal-equilibrium population density in the state l:

$$N_l = \frac{NK_{l'l}}{K_{ll'}+K_{l'l}} . \tag{A12}$$

The result (A11) can also be independently derived from the general result involving upper- (g_u) and lower- (g_l) state degeneracies,

$$\int \alpha(\omega_L) d\omega_L = N_l \lambda^2 \gamma_u g_u / 4 g_l .$$

Finally, theoretical values of the parameters needed for Sec. VI are obtained from

$$C = \alpha_0 LF/2\pi , \tag{A13}$$

where C is the cooperativity (see, e.g., Ref. 41), L is the effective absorption length (Sec. V A 2), and F is the cavity finesse for zero vapor pressure (Sec. IV A), and from

$$Y_+ = Y_- = \frac{1}{\sqrt{2}} Y , \tag{A14}$$

where $Y=X$ under the special conditions of an empty (zero Sm vapor pressure) exactly resonant cavity.

*Permanent address: University of Otago, Dunedin, New Zealand.

[1]H. M. Gibbs, *Optical Bistability: Controlling Light with Light* (Academic, Orlando, FL, 1985).
[2]C. Parigger, P. Hannaford, W. J. Sandle, and R. J. Ballagh, Phys. Rev. A **31**, 4043 (1985).
[3]M. Kitano, T. Yabuzaki, and T. Ogawa, Phys. Rev. Lett. **46**, 926 (1981).
[4]M. W. Hamilton, R. J. Ballagh, and W. J. Sandle, Z. Phys. B **49**, 263 (1982).
[5]C. M. Savage, H. J. Carmichael, and D. F. Walls, Opt. Commun. **42**, 211 (1982).
[6]S. Cecchi, G. Giusfredi, E. Petriella, and P. Salieri, Phys. Rev. Lett. **49**, 1928 (1982).
[7]M. W. Hamilton, W. J. Sandle, J. T. Chilwell, J. S. Satchell, and D. M. Warrington, Opt. Commun. **48**, 190 (1983).
[8]J. Mlynek, F. Mitschke, R. Deserno, and W. Lange, Phys. Rev. A **29**, 1297 (1984).
[9]G. Giusfredi, P. Salieri, S. Cecchi, and F. T. Arecchi, Opt. Commun. **54**, 39 (1985).
[10]E. Giacobino, Opt. Commun. **56**, 249 (1985).
[11]W. E. Schulz, W. R. MacGillivray, and M. C. Standage, Opt. Commun. **45**, 67 (1983).
[12]E. Arimondo and G. Orriols, Lett. Nuovo Cimento **17**, 333 (1976); G. Orriols, Nuovo Cimento **53B**, 1 (1979).
[13]See, e.g., R. J. McLean, R. J. Ballagh, and D. M. Warrington, J. Phys. B **18**, 2371 (1985).
[14]M. Ducloy, Phys. Rev. A **9**, 1319 (1974).
[15]D. F. Walls and P. Zoller, Opt. Commun. **34**, 260 (1980).
[16]F. T. Arecchi, J. Kurmann, and A. Politi, Opt. Commun. **44**, 421 (1983).
[17]J. Mlynek, F. Mitschke, R. Deserno, and W. Lange, Appl. Phys. B **28**, 135 (1982).
[18]F. Mitschke, J. Mlynek, and W. Lange, Phys. Rev. Lett. **50**, 1660 (1983).
[19]G. P. Agrawal, Phys. Rev. A **29**, 994 (1984).

[20]N. D. Bhaskar and A. Lurio, Phys. Rev. A **13**, 1484 (1976).
[21]R. J. Ballagh and V. Jain, Philos. Trans. R. Soc. London, Ser. A **313**, 445 (1984).
[22]A. Omont, Prog. Quantum Electron. **5**, 69 (1977).
[23]P. Hannaford, Contemp. Phys. **24**, 251 (1983).
[24]Coherent-Radiation-Model CR 699-21.
[25]D. S. Gough, P. Hannaford, R. M. Lowe, and R. J. McLean (unpublished).
[26]D. S. Gough and P. Hannaford, Opt. Commun. **55**, 91 (1985).
[27]H. Kogelnik and T. Li, Appl. Opt. **5**, 1550 (1966).
[28]W. J. Sandle in *Laser Physics,* proceedings of the Second New Zealand Summer School in Laser Physics, edited by D. F. Walls and J. D. Harvey (Academic, Sydney, 1980), pp. 225–239.
[29]Type EMI 9317.
[30]At the Commonwealth Scientific and Industrial Research Organization laboratories, Melbourne, Australia.
[31]H. Brand, B. Nottbeck, H. H. Schulz, and A. Steudel, J. Phys. B **11**, L99 (1978).
[32]W. J. Childs and L. S. Goodman, Phys. Rev. **6**, 2011 (1972).
[33]R. J. Ballagh and C. Parriger, in *Optical Bistability 3,* proceedings of the Third OSA Topical Meeting on Optical Bistability, December 2–4, 1985, edited by H. M. Gibbs, P. Mandel, N. Peyghambarian, and S. D. Smith (Springer-Verlag, Berlin, 1986); C. Parigger and R. J. Ballagh (unpublished).
[34]A. R. Striganov, V. A. Katulin, and V. V. Eliseev, Opt. Spektrosk. **12**, 171 (1962) [Opt. Spectrosc. (U.S.S.R.) **12**, 91 (1962)].
[35]F. Rosebury, *Handbook of Electron Tube and Vacuum Techniques* (Addison-Wesley, Reading, MA, 1965).
[36]P. Hannaford and R. M. Lowe, J. Phys. B **18**, 2365 (1985).
[37]J. Mlynek and W. Lange, Opt. Commun. **30**, 337 (1979).
[38]C. Bréchignac, R. Vetter, and P. R. Berman, J. Phys. B **10**, 3443 (1977).
[39]A. Corney, *Atomic and Laser Spectroscopy* (Clarendon, Oxford, 1977).
[40]P. R. Berman and W. E. Lamb, Jr., Phys. Rev. **187**, 221 (1969).
[41]W. J. Sandle and A. Gallagher, Phys. Rev. A **24**, 2017 (1981).
[42]R. J. Ballagh (private communication).
[43]S. Pancharatnam, Proc. R. Soc. London, Ser. A **330**, 271 (1972).
[44]R. J. Ballagh, J. Cooper, M. W. Hamilton, W. J. Sandle, and D. M. Warrington, Opt. Commun. **37**, 143 (1981).
[45]A. T. Rosenberger, L. A. Orozco, and H. J. Kimble, in *Fluctuations and Sensitivity in Non-Equilibrium Systems,* edited by W. Horsthemke and D. K. Kondepudi (Springer-Verlag, Berlin, 1984); Opt. Commun. (to be published).
[46]A. T. Rosenberger, L. A. Orozco, and H. J. Kimble, Opt. Commun. (to be published).
[47]These equations are generalizations, to include collisional coupling to additional states u',l' of equations essentially as given in Ref. 14.
[48]R. J. Ballagh, J. Cooper, and W. J. Sandle, J. Phys. B **14**, 3881 (1981).
[49]J. Cooper and R. J. Ballagh, Phys. Rev. A **18**, 1302 (1978).
[50]The radiative lifetime of the $4f^6 6s\,6p\,{}^7F_1^o$ state (a candidate for u') is 157 ns (see Ref. 36).